Heliyon 10 (2024) e27295

Contents lists available at ScienceDirect

Heliyon

journal homepage: www.cell.com/heliyon

Research article

Intraventricular dimethyl sulfoxide (DMSO) induces hydrocephalus in a dose-dependent pattern

Leandro Castaneyra-Ruiz [a,*], Jenna Ledbetter [a], Seunghyun Lee [a], Anthony Rangel [a], Evelyn Torres [a], Bianca Romero [b], Michael Muhonen [b]

[a] CHOC Children's Research Institute, Orange, CA, 92868, USA
[b] Neurosurgery Department at CHOC Children's Hospital, Orange, CA, 92868, USA

A B S T R A C T

Introduction: Dimethyl sulfoxide (DMSO), a widely utilized solvent in the medical industry, has been associated with various adverse effects, even at low concentrations, including damage to mitochondrial integrity, altered membrane potentials, caspase activation, and apoptosis. Notably, therapeutic molecules for central nervous system treatments, such as embolic agents or some chemotherapy drugs that are dissolved in DMSO, have been associated with hydrocephalus as a secondary complication. Our study investigated the potential adverse effects of DMSO on the brain, specifically focusing on the development of hydrocephalus and the effect on astrocytes.

Methods: Varied concentrations of DMSO were intraventricularly injected into 3-day-old mice, and astrocyte cultures were exposed to similar concentrations of DMSO. After 14 days of injection, magnetic resonance imaging (MRI) was employed to quantify the brain ventricular volumes in mice. Immunofluorescence analysis was conducted to delineate DMSO-dependent effects in the brain. Additionally, astrocyte cultures were utilized to assess astrocyte viability and the effects of cellular apoptosis.

Results: Our findings revealed a dose-dependent induction of ventriculomegaly in mice with 2%, 10%, and 100% DMSO injections ($p < 0.001$). The ciliated cells of the ventricles were also proportionally affected by DMSO concentration ($p < 0.0001$). Furthermore, cultured astrocytes exhibited increased apoptosis after DMSO exposure ($p < 0.001$).

Conclusion: Our study establishes that intraventricular administration of DMSO induces hydrocephalus in a dose-dependent manner. This observation sheds light on a potential explanation for the occurrence of hydrocephalus as a secondary complication in intracranial treatments utilizing DMSO as a solvent.

1. Introduction

Dimethyl sulfoxide (DMSO) is a polar aprotic organic solvent exhibiting high water affinity and is widely used to dissolve small hydrophobic drugs for therapeutic use [1]. DMSO is also used as cryoprotectant [1,2] and is associated with anti-inflammatory and analgesic properties, making it a potential treatment for various medical conditions, including arthritis, interstitial cystitis, and systemic sclerosis [3,4]. Additionally, it has been suggested that DMSO can provide neuroprotective effects, acting as an antioxidant that neutralizes free radicals [5,6]. The accepted low toxicity at concentrations <10% has resulted in the extensive use of DMSO in the pharmaceutical industry [7]. However, DMSO-dependent microRNAs changes and alterations in the epigenetic landscape have been reported to impact cellular viability through mitochondrial damage and caspase-dependent apoptosis. Even a low-concentration dose (2–4 %) [7,8]. DMSO is often used as a solvent for chemotherapy drugs for brain tumors, such as temozolomide (TMZ) [9–11], a drug to treat gliomas [12], and methotrexate, which is often injected intraventricularly or intrathecally to treat leptomeningeal metastasis [13] and also, intravenously to treat pediatric gliomas [14]. Reports of communicating hydrocephalus following glioma treatment

* Corresponding author.
E-mail address: Leandro.Castaneyra.Ruiz@choc.org (L. Castaneyra-Ruiz).

https://doi.org/10.1016/j.heliyon.2024.e27295
Received 6 September 2023; Received in revised form 26 February 2024; Accepted 27 February 2024
Available online 4 March 2024

without mechanical CSF obstruction have been described in 5–8% of cases. Thus, the pathophysiology of this complication in these cases remains unclear [15,16]. In addition, embolic agents such as onyx or PHIL are dissolved in DMSO, and often the patients exhibit hydrocephalus as a complication after treatment [17,18].

Hydrocephalus is a medical condition in which the ventricular system of the brain becomes enlarged, associated with an

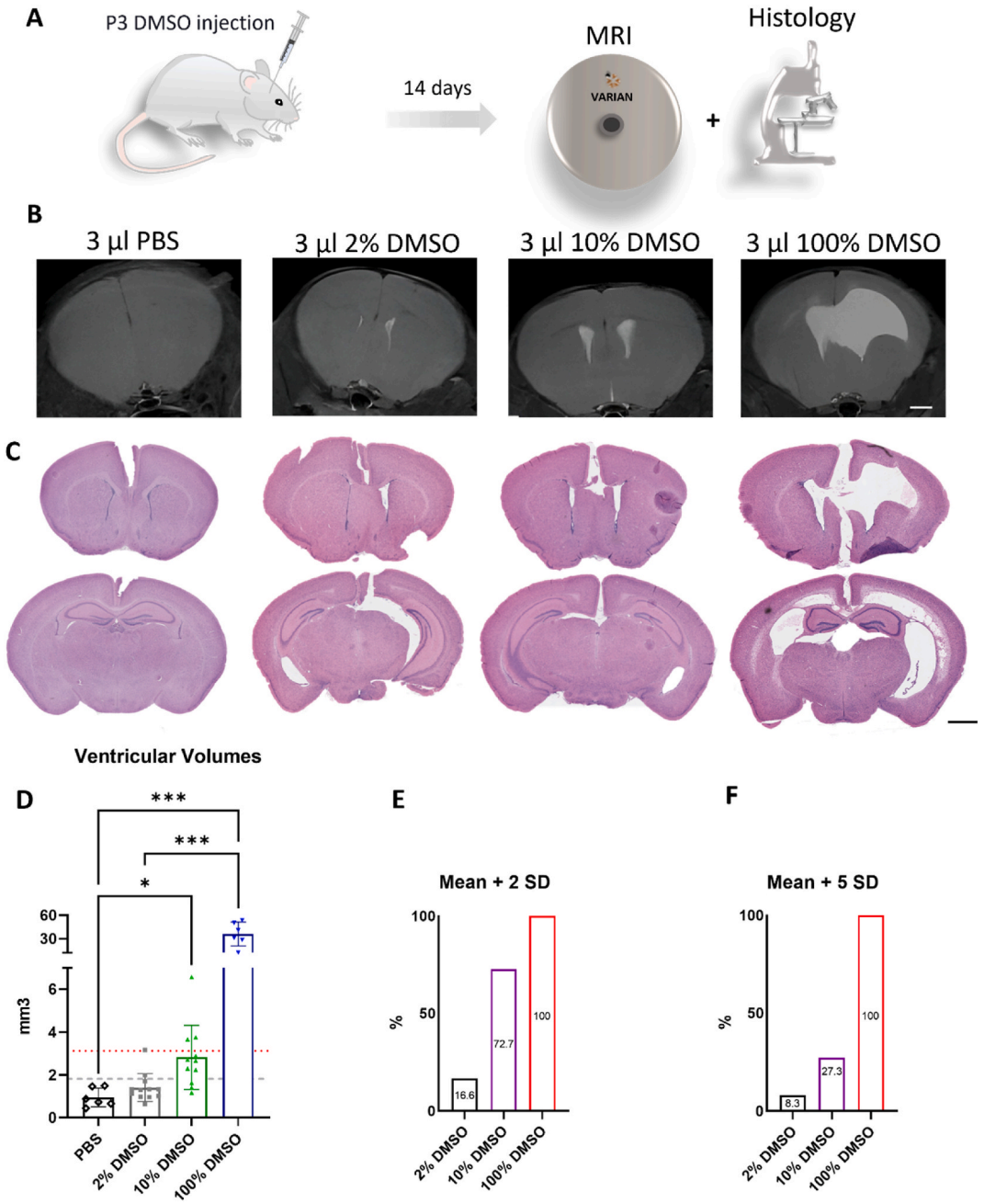

Fig. 1. DMSO induces ventriculomegaly in a dose-dependent pattern. (A) Graphic representation of the experimental design. (B) MRI images indicating the ventricular frontal horn associated with different concentrations of DMSO and the control group. Scale bar, 1 mm. (C) Histological images of the areas of interest labeled with H&E show the lateral ventricles at the prefrontal and parietal levels. Scale bar, 1 mm (D) Ventricular volume quantification (* $p < 0.05$, *** $p < 0.001$, One-way ANOVA with posthoc Tukey test. The box represents the mean, and whiskers denote ± SD. The gray dashed line indicates the mean plus 2 standard deviations of control mice, and the red dotted line indicates the mean plus 5 standard deviations). (E) Percentages of mice with ventriculomegaly (mice with larger ventricles than mean ventricular size plus two standard deviations of control mice). (F) Percentages of mice with ventriculomegaly (mice with larger ventricles than mean ventricular size + 5 standard deviations of control mice). (For interpretation of the references to colour in this figure legend, the reader is referred to the Web version of this article.)

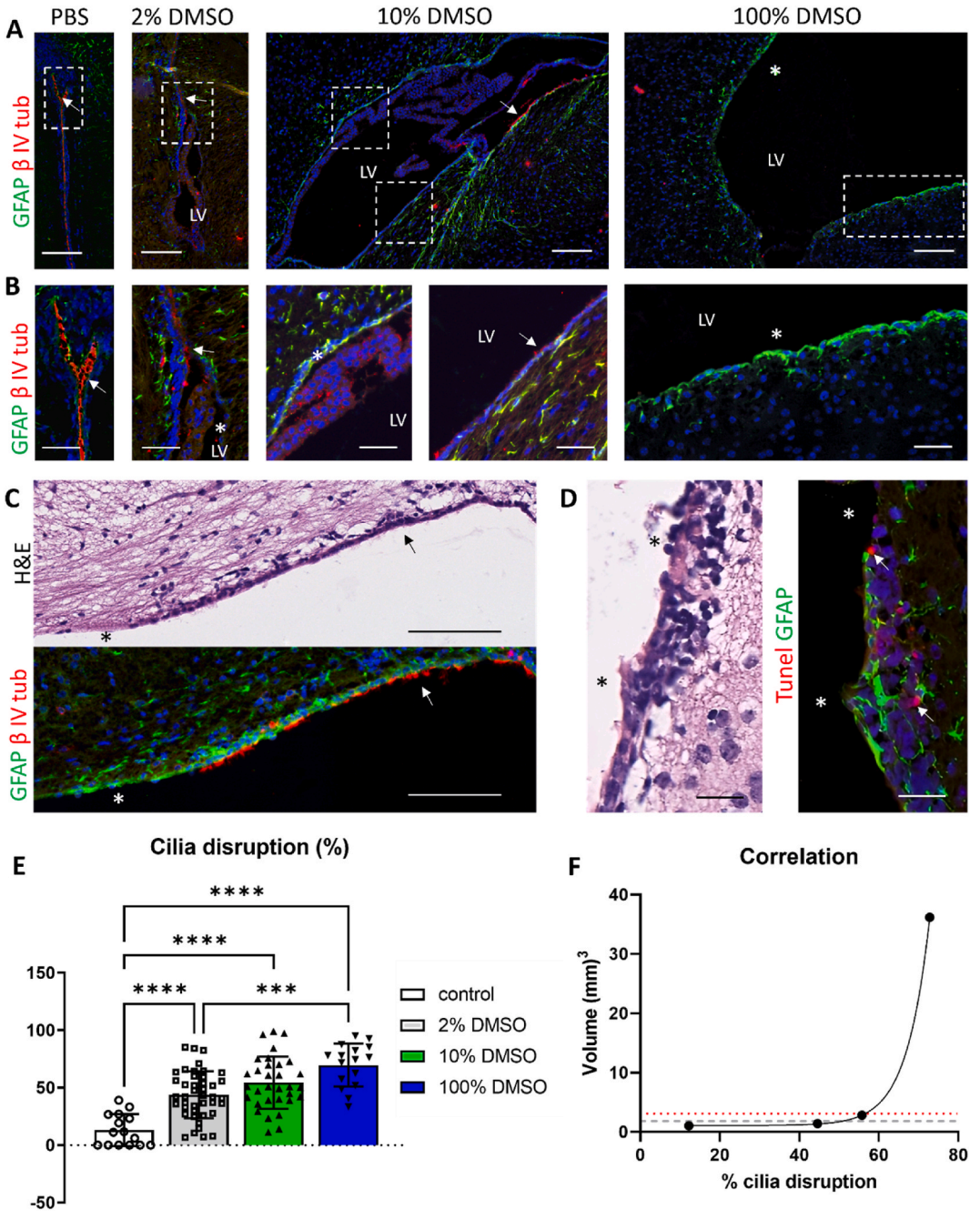

Fig. 2. DMSO-injected mice show a dose-dependent ventricular lining disruption. (A) Representative immunofluorescence of the ventricular lining with the cilia marker anti-βIV tubulin (red) and the astrocyte marker anti-GFAP (green). Scale bars 150 μm. (B) Magnifications of the dashed squares in A. Arrows indicate continuity in the ciliated cells, and asterisks indicate disrupted areas. Scale bars 50 μm. (C) Representative images labeled with H&E (top) and anti-GFAP and anti-βIV tubulin showing ventricular lining disruption (asterisk) in the frontal horn of the lateral ventricles adjacent to an area with normal ciliated cells (arrow). Scale bar, 150 μm. (D) Representative images indicating labeled with H&E (left) and anti-GFAP and anti-βIV tubulin and TUNEL, indicating apoptosis activation (arrows) in the periventricular area adjacent to the ventricular lining disruption (asterisk). Scale bars 20 μm (E) Percentage of ciliated lining disruption (*** $p < 0.001$, **** $p < 0.0001$, One-way ANOVA with posthoc Tukey test. Box represents mean, and whiskers denote ± SD). (F) Correlation between ventricular lining disruption and ventricular volume. The gray dashed line indicates the control ventricular volume mean plus 2 standard deviations, and the red dotted line indicates the mean plus 5 standard deviations. (For interpretation of the references to colour in this figure legend, the reader is referred to the Web version of this article.)

accumulation of cerebrospinal fluid (CSF) and increased intracranial pressure due to the inadequate flow of cerebrospinal fluid (CSF) from the ventricular system to the systemic circulation [19]. One of the main etiologic factors in developing pediatric hydrocephalus is the ventricular zone (VZ) disruption. The VZ is a transient layer in which the radial glial cells (RGC) differentiate into ependymal cells (EC). In mice it is present until ~ postnatal day 15, when all the RGC has differentiated into EC [20]. The multiciliated EC is responsible for the local CSF flow. Therefore, the lack of these cells leads to alterations in the CSF flow and, subsequently, to hydrocephalus [21–25]. Under congenital alterations, such as mutations on alpha snap, or non-genetic conditions, such as intraventricular hemorrhage, the VZ is associated with cell junction alterations that induce the disconnection and subsequent detachment of RGC/EC that are replaced by astrocytes [26–33]. In addition, pathological differentiation of RGC into astrocytes instead of into EC is characteristic in pediatric hydrocephalus, contributing to the lack of EC [26,34–36]. Thus, the loss of RGC is associated with neural migration disorders,

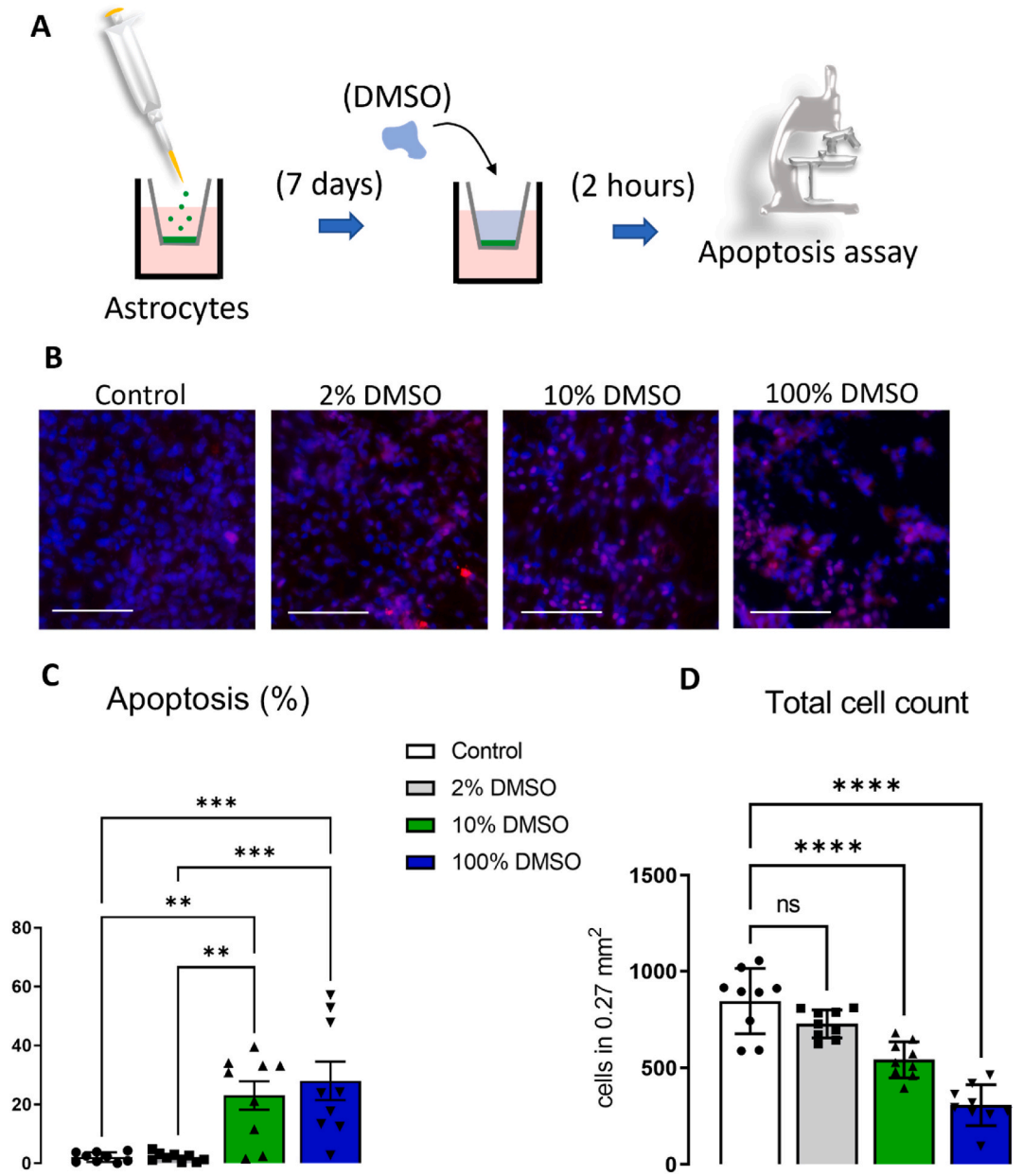

Fig. 3. DMSO induces a dose-dependent apoptosis in astrocyte cultures. (A) Schematic overview of the experimental design (B) Representative images indicating the total cell count labeled with DAPI (blue) and the cells in apoptosis marked with a TUNEL assay (red). Scale bar, 100 μm. (C) Percentage of apoptosis increases significantly at 10 and 100% of DMSO concentration. Quantification (** $p < 0.01$, *** $p < 0.001$, One-way ANOVA with posthoc Tukey test. The box represents the mean, and whiskers denote ± SD). (D) Graphic representation of the cell count associated with DMSO concentration. (**** $p < 0.0001$, One-way ANOVA with posthoc Tukey test. The box represents the mean, and whiskers denote ± SD). (For interpretation of the references to colour in this figure legend, the reader is referred to the Web version of this article.)

including heterotopies and white matter alterations, as previously described in pediatric hydrocephalus [32,37]. Notably, the lack of EC is associated with CSF flow alterations and hydrocephalus. Astrocytes are also crucial in the CSF flow since they are the main structural component of the glymphatic system. The glymphatic system is responsible for clearing excess fluid and metabolic waste. The subarachnoid CSF flows through the periarterial space into the parenchyma, mixed with interstitial fluid, and exits the parenchyma through the perivenous space [38]. The astrocyte end-feet limits the perivascular fluid, playing a fundamental role in the glymphatic system. Thus, alterations in the Astrocyte end-feet are associated with the malfunction of the glymphatic system, water balance, and hydrocephalus [39–41].

DMSO changes the water dynamics in cells, inducing "hyperhydration." Thus, DMSO increases the cell's water content by thinning, creating transient pores, or partially disintegrating the cellular membrane, depending on the concentration used [42]. Our primary goal in this manuscript is to report that DMSO induces hydrocephalus, and we hypothesized that it is associated with toxicity in the VZ and Astrocytes as essential components of the CSF pathway.

2. Results

2.1. DMSO increases ventricular size in a dose-dependent pattern

To determine the effects of DMSO on the neural system, 3-day-old C57BL/6 mice were injected intraventricularly with 3 μl of 2%, 10%, or 100% DMSO and phosphate base saline (PBS) for controls. Magnetic resonance images (MRI) and histology were performed 14 days after ventricular injection (Fig. 1A). MRI confirmed enlarged ventricles in a dose-dependent manner. The forebrain ventricles volume was; 0.94 ± 0.44 mm3 in controls, 1.41 ± 0.66 in 2% DMSO, 2.82 ± 1.50 in 10% DMSO and 36.18 ± 15.35 in 100% DMSO (Fig. 1B–D & Supplemental Table 1). Ventriculomegaly was defined as ventricles 2 standard deviations larger than the mean control ventricular volume. We found that 16.6 % of the mice injected with 2% DMSO developed ventriculomegaly (2 out of 12), 72.7 % of the mice injected with 10% DMSO developed ventriculomegaly (8 out of 11), and 100 % of the mice injected with 100% DMSO developed ventriculomegaly (Fig. 1D and E). Even with more conservative definition of ventriculomegaly as mean control plus 5 SD, we found that 8.3 % of the mice injected with 2% DMSO developed ventriculomegaly (1 out 12), 27.3 % of the mice injected with 10% DMSO developed ventriculomegaly (3 out of 11) and 100 % of the mice injected with 100% DMSO developed ventriculomegaly (Fig. 1D and F).

2.2. DMSO-injected mice show dose-dependent ventricular lining disruption

To determine the neurocytological effects after intraventricular DMSO injection, the periventricular area of the frontal horns was analyzed using immunofluorescence with EC cilia (βIV-tubulin) and astrocyte (GFAP) markers.

We found a ventricular lining cilia loss (EC disruption) that progressively increased at higher concentrations of DMSO and was associated with glial activation (Reactive astrogliosis) and apoptosis (Fig. 2). In control cases, 13.20 ± 13.87 % of the ventricular lining was not ciliated and increased to 43.91 ± 20.57 in 2% DMSO, 54.34 ± 22.70 in 10% DMSO, and 69.77 ± 18.69. (Fig. 2E & Supplemental Table 2). Interestingly, there was no linear correlation between lack of ciliated cells and ventricular volume $r = 0.7166$, $p = 0.2834$. The relation between volume and cilia disruption showed an exponential distribution, suggesting that ventriculomegaly takes place (control mean ventricular volume + 2 SD) at ~ 51 % disrupted ventricular lining or at ~58 % disrupted ventricular lining (control mean ventricular volume + 5 SD) (Fig. 2F).

2.3. DMSO induces apoptosis in a dose-dependent manner in astrocyte cultures

To determine if astrocytes, a key component in the VZ disruption due to the reactive astrogliosis associated with hydrocephalus pathology [43] and as a structural component of the glymphatic system involved in the parenchymal CSF pathway [38,44], were affected by increased concentrations of DMSO, transwell astrocyte cultures were performed. Astrocyte viability was evaluated in cell cultures (Fig. 3). Results showed that the astrocytes activate apoptosis significantly at 10% and 100% DMSO concentrations (respectively, 23.08 ± 14.48 and 28.03 ± 19.64 % of the total cell count) when compared with control (2.13 ± 1.65 %) or 2% DMSO (2.15 ± 1.45, $P < 0.0001$) (Fig. 3C & Supplemental Table 3). The cell count decreased with the DMSO concentration. The mean cell count was 846.2 ± 169.5 in control, 728.4 ± 72.65 in 2% DMSO, 542.7 ± 93.08 in 10% DMSO, 307.6 ± 106.0 in 100% DMSO ($P < 0.0001$) (Fig. 3D Supplemental Table 3).

3. Discussion

Although DMSO is associated with well-documented severe side effects, including organ damage and intravascular hemolysis, and mild adverse reactions like nausea, vomiting, hypertension, and allergic responses [45], it remains one of life sciences' most used pharmaceutical products. DMSO is considered a universal solvent exhibiting remarkable efficacy in dissolving polar and nonpolar compounds [1,2]. Our results showed the induction of ventriculomegaly in a DMSO dose-dependent manner. Other authors have reported dose-dependent pernicious effects associated with DMSO on lipid content, cell viability, and oxidative stress, even a low-concentration dose (1 %) [46]. In addition, DMSO-dependent microRNA changes and alterations in the epigenetic landscape have been reported to induce mitochondrial damage and caspase-dependent apoptosis at 2–4 % DMSO [7,8]. Interestingly, at 2% DMSO we found that between 8 and 16 % of the mice developed ventriculomegaly, which is consistent with the percentage of hydrocephalus

complications of unknown etiology found in patients treated with TMZ dissolved in DMSO (~5–8 % of the cases) [15,16] also it could explain why embolic treatments like onyx (dissolved in DMSO) are associated with hydrocephalus as a secondary complication in pediatric patients [17]. In recent years, ventricular zone (VZ) disruption has been described as a fundamental trigger in the pathogenesis of pediatric hydrocephalus [31,32,34,37]. At an early age, the disruption of the ventricular lining impairs the normal multiciliated ependymal cells' (EC) function and development [27,31,35,36,43]. The cilia motion of the EC plays a fundamental role in the movement of CSF adjacent to the ventricular lining. Thus, a lack or malfunction of these cilia is associated with altered CSF flow and ventriculomegaly [21,47]. Our results show a progressive diminution of cilia in the ventricular lining in a DMSO dose-dependent ratio. This is also associated with a layer of astrocytes replacing the EC, as is reported in other animal models and clinical data [31,33,43]. In this report, we propose that the toxicity associated with DMSO alters the cilia expression and viability of the VZ cells, including EC and astrocytes, as our histological preparations show cellular apoptosis in the ventricular lining of the areas with ventricular zone disruption. However, the lack of cilia does not correlate proportionally with the ventriculomegaly quantified with MRI. Therefore, we believe other factors may contribute to the development of hydrocephalus. Such as alterations in the blood-brain or the blood-CSF barriers, besides the described alterations in the ependymal barrier.

We performed confluent astrocyte cultures to confirm if DMSO can induce apoptosis in other neural cells. Astrocytes are associated with VZ disruption and play a fundamental role in the blood-brain barrier permeability [48], which is increased periventricularly in hydrocephalus [49]. Our cell cultures show that astrocytes are highly sensitive to DMSO, mainly at concentrations of 10% DMSO or above, where we found high levels of astrocyte apoptosis that may be associated with the etiopathology of hydrocephalus.

In conclusion, this is the first report that demonstrates DMSO induction of hydrocephalus when injected intraventricularly in perinatal mice, likely due to the toxicity associated with the periventricular areas. Due to the widespread use of DMSO in clinical settings, its potential adverse effects on the brain must be understood by clinicians administrating medications intracranially that are dissolved with DMSO.

4. Limitations of the study

Our studies were limited to our experimental mouse model. Therefore, these results should be carefully considered when extrapolating to humans.

5. STAR★Methods

Key resources table (Table 1).

5.1. Experimental model and subject details

Experimental animals. Subjects utilized in this study comprised wild-type mice (C57BL/6). The pregnant dams were acquired

Table 1
Key resources table. NIH, National Institutes of Health. Cat#, Catalog number.

REAGENT OF RESOURCE	SOURCE	IDENTIFIER
Antibodies		
Mouse Anti-beta IV Tubulin	Abcam	Cat#: ab11315
Rabbit Anti-GFAP	Abcam	Cat#: ab7260
Anti-mouse IgC (H + L)	Sigma	Cat#: SAB4600066
Goat Anti-Rabbit IgC H&L	Abcam	Cat#: ab150077
Chemicals, peptides, and recombinant proteins		
Phosphate buffered saline (PBS)	Gibco	Cat#: 70011-044
Paraformaldehyde	Thermo Scientific	Cat#: J61899
Dimethyl Sulfoxide	Sigma Life Science	Cat#: D2438
Fetal Bovine Serum	ScienCell	Cat#: 0010
Penicillin/streptomycin Solution	ScienCell	Cat#: 0503
fluoromount-G w/DAPI	Invitrogen	Cat#: 00-4959-52
Ethanol	VWR	Cat#: 89370-084
Xylene	Cardinal Health	Cat#: C4330
IHC Select Citrate Buffer	Millipore Sigma	Cat#: 21545
SuperSignal West Pico Chemiluminescent	Thermo Scientific	Cat#: 34577
Astrocyte Growth Supplement	ScienCell	Cat#: 1852
Basal Medium	ScienCell	Cat#: 1801
Laemmli Sample Buffer	Thermo Scientific	Cat#: 84788
Sample Reducing Agent	Novex	Cat#: 2398614
Critical Commercial Assays		
TUNEL Assay Kit-BrdU – Red	Abcam	Cat#: ab66110
Cells		
Human Astrocytes	ScienCell	Cat#: 1800
Software and Systems		
Image J	NIH	https://imagej.en.softonic.com/

from The Jackson Laboratory, which subsequently delivered the pups under the supervision of the Animal Experimentation Service of the Children's Hospital of Orange County. Mice were housed in a controlled environment at 22 °C with a 12:12 light/dark cycle and provided standard food and water ad libitum. All animal handling, care, housing, and experimental procedures adhered to established protocols and legislation. Approval for experimental protocols was obtained from the Children's Hospital in Orange County Institutional Animal Care and Use Committee. Furthermore, experiments were conducted according to guidelines outlined in the Guide for the Care and Use of Laboratory Animals and the Animal Welfare Act within an AAALAC-accredited facility. Three-day-old mice were injected with 3 μL of PBS (n = 6), 2% DMSO in PBS (n = 12), 10% DMSO in PBS (n = 11), or 100% DMSO (n = 6) into the right lateral ventricle following stereotactic coordinates (0.8 mm lateral, 1.7 mm anterior, and 1.5 mm deep from the lambdoid fontanelle) as previously described [50]. The solutions were injected over 30 s using a 25-μL syringe (Hamilton, 80366) with a UMP3 Ultra Micropump (World Precision Instruments) while animal anesthesia was induced through hypothermia.

Magnetic resonance imaging. MRI was conducted 14 days post-DMSO injection, an in vivo MRI was performed, and mice were euthanized for immunohistochemistry analyses. The mice (dam and pups) were transported from CHOC to the Preclinical and Translational Neuroimaging Center at the University of California, Irvine, to perform magnetic resonance imaging. The mice were received by the UC Irvine personnel and treated under the Preclinical and Translational Neuroimaging Center mice protocol (IACUC standing for routine MRI imaging, AUP 20–172; MRI Services). Imaging was conducted using a 4.7T horizontal bore Agilent MRI and a 2 cm ID quadrature RF coil. The animals were administered with isoflurane anesthesia, and their core temperature was regulated through controlled airflow. Respiration was monitored and maintained by adjustments in anesthesia.

T2-weighted images were used for ventricular volume segmentation with the ITK-SNAP program (ITK-SNAP 4.0, www.itksnap.org). The ventricular volume was quantified according to the method described by Botfield et al. (2013) [51].

Cell growth. 1 mL of Human Astrocytes (ScienCell, Cat. #1800) was thawed at 37 °C for 5 min. Complete astrocyte medium was prepared by adding 5 mL of Astrocyte Growth Supplement (AGS, Cat #1852), 10 mL of fetal bovine serum (FBS, Cat. #0010), and 5 mL of penicillin/streptomycin solution (P/S, Cat. #0503) to 500 mL of basal medium (ScienCell, Cat. #1801). The media was warmed to 37 °C. The thawed astrocytes were combined with 2 mL of the media and were seeded onto one 24-well plate (100 μL/well, 33,333 cells/well) and 12- transwell plate (50 μL/inset, 16,666 cells/inset). The cells were incubated for 1 h under standard conditions (37 °C, 5% CO2). After 1 h, additional media was added to the 24-well plate (1mL/well) and the 12-transwell plate (200 μL/inset, 800 μL/well). Cells were then incubated under standard conditions for 7 days, with the media being refreshed every 48 h.

Immunofluorescence. After Imaging, the mice were euthanized through cardiac perfusion at UC Irvine (IACUC protocol AUP 20–172). Under deep general anesthesia (inhaled isoflurane + IP injection of ketamine and xylazine), the chest wall was opened to expose the heart, and 4% paraformaldehyde was injected into the left ventricle. Mice's brains were dissected, dehydrated, embedded in paraffin, and cut coronally in 10-μm thick sections. Tissue samples were deparaffinized and rehydrated using three Xylene incubations followed by three ethanol incubations (100%, 95%, and 70%). One slide of each brain was stained with hematoxylin and eosin (H&E), and adjacent slices were used for immunoreaction. The cuts were treated with IHC Select Citrate Buffer for 20 min at 100 C°. Then slides were washed in dH2O minutes and PBS for 5 min each. Tissue samples were covered with primary antibodies Anti-Beta IV Tubulin at 1:100 (Abcam, AB11315) and Anti-GFAP at 1:400 (Abcam, AB7260). After 24 h of incubation at room temperature, tissue was covered with fluorescent anti-mouse (1:400) and fluorescent anti-rabbit (1:400) secondary antibodies for 2 h. After two 5-min PBS washes, samples were treated with fluoromount-G, DAPI mounting solution, and coverslipped.

The immunofluorescence was imaged using a KEYENCE microscope. The percentage of ciliated ventricular lining was quantified in the axial plane of the frontal horns. Thus, the length of the non-ciliated ventricular lining was divided by the total length of the ventricular lining and multiplied by 100.

In vitro apoptosis assay. Cells were incubated with different DMSO solutions at 2% (15.3 μL DMSO + 749.7 μL media), 10% (76.5 μL DMSO + 688.5 μL media), and 100% (765 μL DMSO). PBS was used as a control (765 μL PBS). Additional media (9 mL) was added to each solution. Every 1 mL of the 100% DMSO solution contained 85 μL of DMSO. Cells were treated with the DMSO solutions for a period of 2 h before undergoing immunofluorescence.

s for 2 h. After 2 h, cells were rinsed in two 5-min PBS washes. Cells were then fixed with paraformaldehyde for 7 min, which was followed by 2 5-min washes in PBS. Cells were stained using TUNEL Assay Kit -BrdU-Red (Abcam, ab66110). The membrane of the inserts was removed and mounted using fluoromount-G with DAPI mounting solution (Thermofisher, 00-4959-52). The fluorescence was imaged using a KEYENCE microscope. The total cells were quantified through DAPI labeling (blue) as previously described [35,52,53]. Similarly, the apoptosis was quantified trough tunnel labeling (red). The NIH software, ImageJ was used to perform these quantifications.

Statistical analysis. Analyses were performed using GraphPad Prism 9 Software (San Diego, CA, USA). Data were represented as mean ± SD. Kolmogorov-Smirnov test was used to confirm normality ($P > 0.1$) and one way ANOVA with posthoc Tuckey test was used to analyze the data. Comparisons were considered statistically significant at $p < 0.05$.

Data and code availability

This paper does not report new code. Any additional data can be provided by the corresponding author.

Data availability

All data supporting the results in this manuscript are included in the supplemental materials.

Further information can be requested from the corresponding author contact, Dr. Leandro Castaneyra-Ruiz (Leandro.castaneyra.

ruiz@choc.org).

Ethics statement

The animal protocols were authorized by the Institutional Animal Care and Use Committee at Children's Hospital in Orange County, and the experiments were conducted in a facility accredited by AAALAC, adhering to the guidelines outlined in the Guide for the Care and Use of Laboratory Animals and the Animal Welfare Act, under the approval number 210679.

CRediT authorship contribution statement

Leandro Castaneyra-Ruiz: Writing – review & editing, Writing – original draft, Project administration, Methodology, Investigation, Funding acquisition, Conceptualization. **Jenna Ledbetter:** Investigation, Formal analysis, Data curation. **Seunghyun Lee:** Visualization, Software, Methodology, Investigation, Formal analysis. **Anthony Rangel:** Methodology, Investigation. **Evelyn Torres:** Methodology, Investigation. **Bianca Romero:** Resources, Methodology. **Michael Muhonen:** Supervision, Project administration, Investigation, Funding acquisition, Conceptualization.

Declaration of generative AI and AI-assisted technologies in the writing process

The authors employed Grammarly and Chat GPT to enhance the language and readability of the manuscript. Subsequently, the authors thoroughly reviewed and edited the document and assumed complete responsibility for the publication's content.

Declaration of competing interest

The authors declare that they have no known competing financial interests or personal relationships that could have appeared to influence the work reported in this paper.

Acknowledgments

This work was supported by a fund provided by the CHOC foundation, CSO Small Grants Program, 2022, awarded by L.C.-R, and The LeVecke Family Foundation through a donation to CHOC Children's Hospital.

Appendix A. Supplementary data

Supplementary data to this article can be found online at https://doi.org/10.1016/j.heliyon.2024.e27295.

References

[1] C.F. Brayton, Dimethyl sulfoxide (DMSO): a review, Cornell Vet. Jan 76 (1) (1986) 61–90.
[2] P.V. Dludla, B.B. Nkambule, S.E. Mazibuko-Mbeje, et al., The impact of dimethyl sulfoxide on oxidative stress and cytotoxicity in various experimental models. Toxicology, Elsevier, 2021, pp. 243–261.
[3] M. Colucci, F. Maione, M.C. Bonito, A. Piscopo, A. Di Giannuario, S. Pieretti, New insights of dimethyl sulphoxide effects (DMSO) on experimental in vivo models of nociception and inflammation, Pharmacol Res. Jun 57 (6) (2008) 419–425, https://doi.org/10.1016/j.phrs.2008.04.004.
[4] A.L. Scherbel, Multiclinic study of DMSO for systemic sclerosis, Arthritis Rheum. Dec 28 (12) (1985) 1437–1438, https://doi.org/10.1002/art.1780281221.
[5] A.M. Di Giorgio, Y. Hou, X. Zhao, B. Zhang, B.G. Lyeth, M.J. Russell, Dimethyl sulfoxide provides neuroprotection in a traumatic brain injury model, Restor. Neurol. Neurosci. 26 (6) (2008) 501–507.
[6] C. Sanmartín-Suárez, R. Soto-Otero, I. Sánchez-Sellero, E. Méndez-Álvarez, Antioxidant properties of dimethyl sulfoxide and its viability as a solvent in the evaluation of neuroprotective antioxidants, J. Pharmacol. Toxicol. Methods 63 (2) (2011) 209–215.
[7] J. Galvao, B. Davis, M. Tilley, E. Normando, M.R. Duchen, M.F. Cordeiro, Unexpected low-dose toxicity of the universal solvent DMSO, FASEB J. Mar 28 (3) (2014) 1317–1330, https://doi.org/10.1096/fj.13-235440.
[8] M. Verheijen, M. Lienhard, Y. Schrooders, et al., DMSO induces drastic changes in human cellular processes and epigenetic landscape in vitro, Sci Rep. Mar 15 9 (1) (2019) 4641, https://doi.org/10.1038/s41598-019-40660-0.
[9] P. McConville, D. Hambardzumyan, J.B. Moody, et al., Magnetic resonance imaging determination of tumor grade and early response to temozolomide in a genetically engineered mouse model of glioma, Clin. Cancer Res. 13 (10) (May 15 2007) 2897–2904, https://doi.org/10.1158/1078-0432.CCR-06-3058.
[10] L. Tentori, C. Leonetti, M. Scarsella, et al., Systemic administration of GPI 15427, a novel poly(ADP-ribose) polymerase-1 inhibitor, increases the antitumor activity of temozolomide against intracranial melanoma, glioma, lymphoma, Clin Cancer Res. Nov 1 9 (14) (2003) 5370–5379.
[11] B. Yamini, X. Yu, P. Pytel, et al., Adenovirally delivered tumor necrosis factor-alpha improves the antiglioma efficacy of concomitant radiation and temozolomide therapy, Clin. Cancer Res. 13 (20) (Oct 15 2007) 6217–6223, https://doi.org/10.1158/1078-0432.CCR-07-1421.
[12] Z. Hu, Y. Mi, H. Qian, et al., A potential mechanism of temozolomide resistance in glioma-ferroptosis, Front. Oncol. 10 (2020) 897, https://doi.org/10.3389/fonc.2020.00897.
[13] E. Le Rhun, M. Weller, D. Brandsma, et al., EANO-ESMO Clinical Practice Guidelines for diagnosis, treatment and follow-up of patients with leptomeningeal metastasis from solid tumours, Ann. Oncol. 28 (suppl_4) (Jul 1 2017) iv84–iv99, https://doi.org/10.1093/annonc/mdx221.
[14] J.E. Wolff, R.D. Kortmann, B. Wolff, et al., High dose methotrexate for pediatric high grade glioma: results of the HIT-GBM-D pilot study, J Neurooncol. May 102 (3) (2011) 433–442, https://doi.org/10.1007/s11060-010-0334-2.
[15] C.M. Fischer, M.C. Neidert, D. Peus, et al., Hydrocephalus after resection and adjuvant radiochemotherapy in patients with glioblastoma, Clin. Neurol. Neurosurg. 120 (May 2014) 27–31, https://doi.org/10.1016/j.clineuro.2014.02.012.

[16] N. Montano, Q.G. D'Alessandris, F. Bianchi, et al., Communicating hydrocephalus following surgery and adjuvant radiochemotherapy for glioblastoma, J Neurosurg. Dec 115 (6) (2011) 1126–1130, https://doi.org/10.3171/2011.8.JNS11738.
[17] R. Chen, S. Zhang, C. You, R. Guo, L. Ma, Pediatric intracranial aneurysms: changes from previous studies, Childs Nerv Syst. Sep 34 (9) (2018) 1697–1704, https://doi.org/10.1007/s00381-018-3818-6.
[18] D. Brown, C. Graham, A. Smith, et al., Same day embolisation followed by microsurgical resection of brain arteriovenous malformations: a single centre early experience, Br J Neurosurg. Feb 35 (1) (2021) 80–83, https://doi.org/10.1080/02688697.2020.1765972.
[19] H.L. Rekate, A contemporary definition and classification of hydrocephalus, Semin Pediatr Neurol. Mar 16 (1) (2009) 9–15, https://doi.org/10.1016/j.spen.2009.01.002.
[20] N. Delgehyr, A. Meunier, M. Faucourt, et al., Ependymal cell differentiation, from monociliated to multiciliated cells, Methods Cell Biol. 127 (2015) 19–35, https://doi.org/10.1016/bs.mcb.2015.01.004.
[21] K. Abdi, C.H. Lai, P. Paez-Gonzalez, M. Lay, J. Pyun, C.T. Kuo, Uncovering inherent cellular plasticity of multiciliated ependyma leading to ventricular wall transformation and hydrocephalus, Nat. Commun. 9 (1) (Apr 25 2018) 1655, https://doi.org/10.1038/s41467-018-03812-w.
[22] C. Gavino, S. Richard, Patched 1 haploinsufficiency impairs ependymal cilia function of the quaking viable mice, leading to fatal hydrocephalus, Mol Cell Neurosci. Jun 47 (2) (2011) 100–107, https://doi.org/10.1016/j.mcn.2011.03.004.
[23] W. Zou, Y. Lv, Z.I. Liu, P. Xia, H. Li, J. Jiao, Loss of Rsph9 causes neonatal hydrocephalus with abnormal development of motile cilia in mice, Sci. Rep. 10 (1) (Jul 24 2020) 12435, https://doi.org/10.1038/s41598-020-69447-4.
[24] C. Wodarczyk, I. Rowe, M. Chiaravalli, M. Pema, F. Qian, A. Boletta, A novel mouse model reveals that polycystin-1 deficiency in ependyma and choroid plexus results in dysfunctional cilia and hydrocephalus, PLoS One 4 (9) (Sep 23 2009) e7137, https://doi.org/10.1371/journal.pone.0007137.
[25] S. Ohata, J. Nakatani, V. Herranz-Perez, et al., Loss of Dishevelleds disrupts planar polarity in ependymal motile cilia and results in hydrocephalus, Neuron 83 (3) (Aug 6 2014) 558–571, https://doi.org/10.1016/j.neuron.2014.06.022.
[26] L. Castaneyra-Ruiz, I. Gonzalez-Marrero, L.G. Hernandez-Abad, et al., AQP4 labels a subpopulation of white matter-dependent glial radial cells affected by pediatric hydrocephalus, and its expression increased in glial microvesicles released to the cerebrospinal fluid in obstructive hydrocephalus, Acta Neuropathol Commun. Mar 28 10 (1) (2022) 41, https://doi.org/10.1186/s40478-022-01345-4.
[27] M. Garcia-Bonilla, L. Castaneyra-Ruiz, S. Zwick, et al., Acquired hydrocephalus is associated with neuroinflammation, progenitor loss, and cellular changes in the subventricular zone and periventricular white matter, Fluids Barriers CNS 19 (1) (Feb 22 2022) 17, https://doi.org/10.1186/s12987-022-00313-3.
[28] M.R. Del Bigio, Neuropathology and structural changes in hydrocephalus, Dev Disabil Res Rev 16 (1) (2010) 16–22, https://doi.org/10.1002/ddrr.94.
[29] A.M. Isaacs, J.J. Neil, J.P. McAllister, et al., Microstructural periventricular white matter injury in post-hemorrhagic ventricular dilatation, Neurology. Nov 19 (2021), https://doi.org/10.1212/WNL.0000000000013080.
[30] A.M. Isaacs, J.S. Shimony, D.M. Morales, et al., Feasibility of fast brain diffusion MRI to quantify white matter injury in pediatric hydrocephalus, J Neurosurg Pediatr. Jul 19 (2019) 1–8, https://doi.org/10.3171/2019.5.PEDS18596.
[31] R.J. Ferland, L.F. Batiz, J. Neal, et al., Disruption of neural progenitors along the ventricular and subventricular zones in periventricular heterotopia, Hum Mol Genet. Feb 1 18 (3) (2009) 497–516, https://doi.org/10.1093/hmg/ddn377.
[32] M.M. Guerra, R. Henzi, A. Ortloff, et al., Cell junction pathology of neural stem cells is associated with ventricular zone disruption, hydrocephalus, and abnormal neurogenesis, J Neuropathol Exp Neurol. Jul 74 (7) (2015) 653–671, https://doi.org/10.1097/NEN.0000000000000203.
[33] J.P. McAllister, M.M. Guerra, L.C. Ruiz, et al., Ventricular zone disruption in human neonates with intraventricular hemorrhage, J. Neuropathol. Exp. Neurol. 76 (5) (May 1 2017) 358–375, https://doi.org/10.1093/jnen/nlx017.
[34] L. Castaneyra-Ruiz, I. Gonzalez-Marrero, L.G. Hernandez-Abad, S. Lee, A. Castaneyra-Perdomo, M. Muhonen, AQP4, astrogenesis, and hydrocephalus: a new neurological perspective, Int J Mol Sci. Sep 9 (18) (2022) 23, https://doi.org/10.3390/ijms231810438.
[35] L. Castaneyra-Ruiz, D.M. Morales, J.P. McAllister, et al., Blood exposure causes ventricular zone disruption and glial activation in vitro, J Neuropathol Exp Neurol. Sep 1 77 (9) (2018) 803–813, https://doi.org/10.1093/jnen/nly058.
[36] L. Castaneyra-Ruiz, J.P. McAllister 2nd, D.M. Morales, S.L. Brody, A.M. Isaacs, D.D. Limbrick Jr., Preterm intraventricular hemorrhage in vitro: modeling the cytopathology of the ventricular zone, Fluids Barriers CNS 17 (1) (Jul 20 2020) 46, https://doi.org/10.1186/s12987-020-00210-7.
[37] E.M. Rodriguez, M.M. Guerra, K. Vio, et al., A cell junction pathology of neural stem cells leads to abnormal neurogenesis and hydrocephalus, Biol. Res. 45 (3) (2012) 231–242, https://doi.org/10.4067/S0716-97602012000300005.
[38] J.J. Iliff, M. Wang, Y. Liao, et al., A paravascular pathway facilitates CSF flow through the brain parenchyma and the clearance of interstitial solutes, including amyloid β, Sci. Transl. Med. 4 (147) (2012), 147ra111-147ra111.
[39] I. Gonzalez-Marrero, L.G. Hernandez-Abad, M. Gonzalez-Gomez, et al., Altered expression of AQP1 and AQP4 in brain barriers and cerebrospinal fluid may affect cerebral water balance during chronic hypertension, Int J Mol Sci. Oct 14 (20) (2022) 23, https://doi.org/10.3390/ijms232012277.
[40] Z. Ding, X. Fan, Y. Zhang, et al., The glymphatic system: a new perspective on brain diseases, Front. Aging Neurosci. 15 (2023) 1179988, https://doi.org/10.3389/fnagi.2023.1179988.
[41] B.C. Reeves, J.K. Karimy, A.J. Kundishora, et al., Glymphatic system impairment in alzheimer's disease and idiopathic normal pressure hydrocephalus, Trends Mol Med. Mar 26 (3) (2020) 285–295, https://doi.org/10.1016/j.molmed.2019.11.008.
[42] A.A. Gurtovenko, J. Anwar, Modulating the structure and properties of cell membranes: the molecular mechanism of action of dimethyl sulfoxide, J Phys Chem B. Sep 6 111 (35) (2007) 10453–10460, https://doi.org/10.1021/jp073113e.
[43] R. Roales-Bujan, P. Paez, M. Guerra, et al., Astrocytes acquire morphological and functional characteristics of ependymal cells following disruption of ependyma in hydrocephalus, Acta Neuropathol. Oct 124 (4) (2012) 531–546, https://doi.org/10.1007/s00401-012-0992-6.
[44] J.S. Generoso, S. Thorsdottir, A. Collodel, et al., Dysfunctional glymphatic system with disrupted aquaporin 4 expression pattern on astrocytes causes bacterial product accumulation in the CSF during pneumococcal meningitis, mBio 13 (5) (Oct 26 2022) e0188622, https://doi.org/10.1128/mbio.01886-22.
[45] M. Cottler-Fox, M. Montgomery, J. Theus, Collection and processing of marrow and blood hematopoietic stem cells, Hematopoietic Stem Cell Transplantation in, Clinical Practice (2009). https://doi.org/10.1016/B978-0-443-10147-2.50028-X.
[46] P.V. Dludla, B. Jack, A. Viraragavan, et al., A dose-dependent effect of dimethyl sulfoxide on lipid content, cell viability and oxidative stress in 3T3-L1 adipocytes, Toxicol Rep 5 (2018) 1014–1020, https://doi.org/10.1016/j.toxrep.2018.10.002.
[47] Z. Jiang, J. Zhou, X. Qin, et al., MT1-MMP deficiency leads to defective ependymal cell maturation, impaired ciliogenesis, and hydrocephalus, JCI Insight (9) (May 7 2020) 5, https://doi.org/10.1172/jci.insight.132782.
[48] E.G. Knox, M.R. Aburto, G. Clarke, J.F. Cryan, C.M. O'Driscoll, The blood-brain barrier in aging and neurodegeneration, Mol Psychiatry. Jun 27 (6) (2022) 2659–2673, https://doi.org/10.1038/s41380-022-01511-z.
[49] M.R. Del Bigio, I. Slobodian, A.E. Schellenberg, R.J. Buist, T.L. Kemp-Buors, Magnetic resonance imaging indicators of blood-brain barrier and brain water changes in young rats with kaolin-induced hydrocephalus, Fluids Barriers CNS 8 (Aug 11 2011) 22, https://doi.org/10.1186/2045-8118-8-22.
[50] J.Y. Kim, S.D. Grunke, Y. Levites, T.E. Golde, J.L. Jankowsky, Intracerebroventricular viral injection of the neonatal mouse brain for persistent and widespread neuronal transduction, J Vis Exp. Sep 15 (91) (2014) 51863, https://doi.org/10.3791/51863.
[51] H. Botfield, A.M. Gonzalez, O. Abdullah, et al., Decorin prevents the development of juvenile communicating hydrocephalus, Brain. Sep 136 (Pt 9) (2013) 2842–2858, https://doi.org/10.1093/brain/awt203.
[52] L. Castaneyra-Ruiz, S. Lee, A.Y. Chan, et al., Polyvinylpyrrolidone-Coated catheters decrease astrocyte adhesion and improve flow/pressure performance in an invitro model of hydrocephalus, Children 10 (1) (Dec 22 2022), https://doi.org/10.3390/children10010018.
[53] S. Lee, J. Ledbetter, J. Davies, B. Romero, M. Muhonen, L. Castaneyra-Ruiz, Polyvinylpyrrolidone-coated catheters decrease choroid plexus adhesion and improve flow/pressure performance in an in vitro model of hydrocephalus, Child's Nerv. Syst. (2023) 1–7.